EUROPEAN ORGANIZATION FOR NUCLEAR RESEARCH

CERN-PPE/91-118
30 July 1991

Observation of Meson Central Production in Baryon Exchange Processes

V. F. Perepelitsa[4], A. Ferrer[3], A. A. Grigoryan[1], P. Sonderegger[2], S. Ya. Nikitin[4]

Abstract

The central production of ρ^0, f_2 and ρ_3^0 mesons is observed for the first time in processes which are originated by $\pi^+ p$ reactions proceeding via baryon exchange mechanism. The data come from the CERN WA56 experiment designed to separate the baryon exchange reactions in $\pi^+ p$−collisions at 20 GeV/c. We report on the measured integral and differential cross sections and also give the density matrix elements of the meson resonances observed.

---

1. Yerevan Physics Institute, Br. Alikhanian st.2, 375036 Yerevan,Armenia,USSR.
2. CERN, 1211 Geneva 23, Switzerland
3. Departamento de Física Atómica Molecular y Nuclear
and IFIC, Univ. of Valencia - CSIC, 46100 Burjassot, Valencia, Spain
4. Institute of Theoretical and Experimental Physics, 117 259 Moscow, USSR.

1. Introduction

Among the hadronic inelastic reactions the reactions referred as "central production" are of special interest. The term central means that the particle (or system of particles) is produced at small values of Feynman variable x, or, equivalently, at small values of the c.m. rapidity, y^*. Central production has been explored for different purposes in the processes which proceed through the exchange of bosonic states in t-channel (see, e.g.,[1]). A diagram which corresponds to such a process in π^+p-collisions is shown in Fig. 1a.

Contrary to boson exchange reactions the central production of hadrons in baryon exchange processes has never been reported before. In this paper we analyze the processes

$$\pi^+p \to p_f M^0 \pi_s^+ \tag{1}$$

where p_f is a fast proton produced with a momentum greater than half of the beam, and M^0 stands for centrally produced vector or tensor mesons ($\rho^0(770), f_2(1270), \rho_3^0(1690)$) decaying into $\pi^+\pi^-$. The corresponding diagram is shown in Fig. 1b.

The data were obtained from the CERN WA56 experiment using the Ω spectrometer. This experiment was originally designed as a high sensitivity search for doubly charged exotic mesons and narrow baryonium states produced via baryon exchange in π^+p interactions at 20 GeV/c [2]. We have analyzed part of the WA56 statistics ($1/\sigma_0 \approx 150$ events per nanobarn out of a total of 427 events per nanobarn) to extract information about non-exotic resonance production proceeding via baryon exchange mechanism. In Ref. [3] we have reported on the results of the analysis of quasi-two-body processes of backward production of mesons $\pi^0, \rho^0, \omega, f_2, \rho_3^0$ together with the $\Delta(1232)$ baryon. Analogous processes were studied previously, mainly at lab momenta $\leq$ 12 GeV/c, see, e.g. the review [4].

The energy of the WA56 experiment is the highest one dealing with multiparticle (n $\geq$ 4) production in baryon exchange processes. This opens a new interesting possibility for investigations in this area: owing to a large rapidity gap between the fastest and the slowest particles of reaction (1) ($\Delta y \approx 5$), it becomes possible to separate and study the central region in the referred reaction.

The paper is organized as follows. In Sect. 2 we describe the experimental set up and the separation of the events of reaction

$$\pi^+p \to p_f \pi^+\pi^-\pi_s^+ \tag{2}$$

related to reaction (1). π_s^+ refers here to the slowest of the two positive pions. The mass spectra of interest are described in Sect. 3. Integral and differential cross sections for ρ^0, f_2, and ρ_3^0 mesons produced centrally via baryon exchange are presented in Sections 4 and 5, and the density matrix elements of the mesons are given in Sect. 6. The comparison of the central production in boson and baryon exchange reactions is done in Sect. 7.

2. Experimental conditions. Selection of events

The layout of the Ω spectrometer as used in the WA56 experiment is shown in Fig. 2. The experiment was designed to enhance the relative yield of baryon exchange reactions with respect to diffractive production of fast forward protons (paired with fast antiprotons). The positively charged beam was focused on a 60 cm long hydrogen target. The incident particles were identified by two Cherenkov counters in the beam. Their momenta and angles were measured by a beam spectrometer and by a set of MWPCs upstream of the target. A 24 element scintillation cylindrical hodoscope ("barrel") surrounding the target and a 1/2 mm pitch wire chamber at its downstream end (Y1 in Fig. 2) provided a measurement of the charged multiplicity. In addition, the barrel information was used to identify the events with slow tracks which were not reconstructed in the off-line treatment. A set of 32 MWPC planes (type C) and of 30 forward MWPC planes (types B and A in Fig. 2) were used to reconstruct the outgoing charged particles. Two drift chambers (DC1 and DC2) were used to improve the measurement accuracy for the fast particles.

The main trigger requirement was the detection of a fast forward proton with momentum greater than 10 GeV/c. The proton signature was determined with the aid of two multicell atmospheric Cherenkov counters C1 and C2 filled with freon-114 and N_2, respectively, and two scintillation hodoscopes H2 and H3 behind them. The momentum of the trigger proton was computed from three proportional planes (Y0, Y3 and Y4 in Fig. 2) providing a rather sharp momentum cut.

Several multiplicity requirements were imposed: $\geq$1 in the barrel hodoscope, $\geq$1 in Y1, $\geq$2 in the two of them, 2 to 5 in proportional plane Y2 and $\leq$3 in Y3. An antiproton veto provided by the C1-H2 system, suppressed the diffractive events with antiprotons of momenta greater than 2.5 GeV/c. A γ veto consisting of hodoscopes H3 and H4 and a lead sheet of 15 mm thickness in between, eliminated the events with fast π^0.

The efficiency of the WA56 set up was not good for slow tracks since side chambers C did not cover the backward hemisfere. The Monte Carlo calculations have shown that the 4-prong acceptance of the WA56 for the reaction (1) was very small (about 0.3%). This feature was confirmed by kinematical processing of the 4-prong events. Therefore, our study of reaction (1) is based on 3-prong events with a $++-$ topology. They were interpreted as coming from 4-prong events where the slowest positive particle was not detected.

The distribution of missing mass squared (MM^2) for these events with appropriate mass hypotheses for the detected particles (the fastest positive track taken as a proton, the rest as pions) is shown in Fig.3a. The mass hypothesis assigned to the tracks was required to be compatible with Cherenkov counter information. A signal of lost π_s^+ is seen there. The signal becomes more clear when requiring that the barrel element associated with the missing momentum gave a signal (fig.3b).

For further analysis we have retained all those $++-$ events which had MM^2 in the m_π^2 band ($|MM^2 - m_\pi^2| \leq 0.16$ $(GeV/c^2)^2$) and which passed a 1-C kinematic fit with $P(\chi^2)$ $\geq$ 5%. The energy-momentum balance obtained with this fit, allowed the reconstruction of 4-momentum of the missed slow pion from reaction (2).

3. Mass spectra. Identification of central production

The $\pi^+\pi^-$ mass spectrum for all selected events shows strong evidence for $\rho^0(770)$ and $f_2(1270)$ production (Fig. 4a). The spectra of rapidities of fast proton, $y^*_{p_f}$, slow pion, $y^*_{\pi_s^+}$, and the $\pi^+\pi^-$ system, $y^*_{\pi^+\pi^-}$ [1] , are plotted in Fig. 5a. A clear separation of the rapidity spectra is seen. Only $\approx 10\%$ of the events have $y^*_{\pi^+\pi^-}$ out of the limits ± 1. The weak overlap among the rapidity spectra is surprising because the WA56 experiment was not designed to separate mesonic states in the central region.

To select more precisely the events of the central production (to ensure $|x_{\pi^+\pi^-}| \leq 0.2$ even in the ρ_3^0 mass region) we have retained the events with $|y^*_{\pi^+\pi^-}| \leq 0.5$ for further analysis. The $\pi^+\pi^-$ mass spectrum for these events is shown in Fig. 4b. In addition to the clearly seen $\rho(770)$ and $f_2(1270)$ signals, some hint for the $\rho_3^0(1690)$ state is visible. An additional cut $M_{p_f\pi^+} \geq 2$ GeV/c^2 improving the $\rho_3^0(1690)$ signal/background ratio increases the evidence for the production of this state (Fig. 4c).

The curves in Fig. 4 are obtained from a parametrization of the mass spectra of the form:

$$(M - M_0)P_3(M)e^{-M}(1 + BW)$$

where M_0 is a constant equal to the mass threshold, P_3 is a 3rd order polynomial and BW means three Breit-Wigner terms with the masses and the widths of ρ^0, f_2, and ρ_3^0 taken from the standard PDG values [5].

4. Integral cross sections

Selecting the events with the following $\pi^+\pi^-$ mass cuts: $|M_{\pi^+\pi^-} - 0.77| \leq 0.12$ GeV/c^2 (ρ^0), $|M_{\pi^+\pi^-} - 1.27| \leq 0.14$ GeV/c^2 (f_2), and $|M_{\pi^+\pi^-} - 1.69| \leq 0.16$ GeV/c^2 (ρ_3^0), and using our mass fit to subtract the background under each resonance peak we have obtained the numbers of ρ^0, f_2 and ρ_3^0 mesons produced centrally via baryon exchange in reaction (1) given in Table 1. Then we have calculated the total acceptances of the experiment for the reaction (1) (where M^0 can take any of the ρ^0, f_2 and ρ_3^0 masses), taking into account the two u' dependences (u'_{p_f} and $u'_{\pi_s^+}$ of Fig. 1b), ρ^0, f_2, ρ_3^0 decay angular distributions extracted from our experimental data (see Sections 5 and 6 below) and cut $M_{p_f\pi^+} \geq 2$ GeV/c^2 in case of ρ_3^0 meson. Combining the acceptances with the numbers of events in each channel we have obtained the integral cross sections given also in Table 1. Note, the cross sections are corrected for the unseen decay modes by multiplying by a factor 1.85 for the f_2 and 4.2 for the ρ_3^0.

[1] The rapidities are defined as usual:

$$y^* = 0.5 ln \frac{E^* + P^*_{||}}{E^* - P^*_{||}}$$

where E* ($P^*_{||}$) is the energy (longitudinal momentum) of the particle or system of particles in the s-channel c.m. frame.

It is interesting to compare the obtained cross sections with the cross sections for backward production of the same mesons in the quasi-two-body processes reported in [3]. Excepting the ρ_3^0 meson the quasi-two-body production has smaller cross sections than central ones. Note also the different behaviour of central and backward cross sections with meson mass: in the latter case there is a regular increase nearly proportional to M^2, while in the former case we observe a fall-off for ρ_3^0 meson. Evidently, this fall-off can be explained by "energetic crisis" affecting the central production at smaller energies than the backward one.

5. Differential cross sections

For each individual channel of the reaction (1) we have plotted two-dimensional distribution of events versus u'_{p_f} and $u'_{\pi_s^+}$ where $u' = u_{max} - u$, and u_{p_f}, $u_{\pi_s^+}$ are squared momentum transfers from the beam particle to p_f and from target to π_s^+, respectively (see Fig. 1b). The distributions were corrected for the u'-dependent acceptances using a Monte Carlo simulation and scaled down by σ_0 giving $\mathrm{d}^2\sigma/\mathrm{d}u'_{p_f}\mathrm{d}u'_{\pi_s^+}$. Projections of these cross sections are shown in Fig.6.

Trying to parametrize these cross sections we have found an essential difference between the u'_{p_f} and $u'_{\pi_s^+}$ distributions for ρ^0 and f_2 channels. The $\mathrm{d}\sigma/\mathrm{d}u'_{p_f}$ can be fitted using a simple exponential form $\mathrm{d}\sigma/\mathrm{d}u'_{p_f} = A_f \exp(-b_f u'_{p_f})$, whereas the $\mathrm{d}\sigma/\mathrm{d}u'_{\pi_s^+}$ can not. We have checked that this difference is neither connected to the acceptance dependence corrections, nor to the background contamination. We have therefore fitted $u'_{\pi_s^+}$ distributions using the expression

$$d\sigma/du'_{\pi_s^+} = A_{s_1} exp(-b_{s_1} u'_{\pi_s^+}) + A_{s_2} u'_{\pi_s^+} exp(-b_{s_2} u'_{\pi_s^+}) \qquad (3)$$

The resulting slopes b_f, b_{s_1}, b_{s_2}, and coefficients A_f, A_{s_1}, A_{s_2} are given in Table 2, and the fitted curves are shown in Fig.6.

Concerning the low statistics ρ_3^0 channel, which was extracted using the strong cut described in Sect. 3, its differential cross section is satisfactoryly fitted with the simple exponential form $\mathrm{d}\sigma/\mathrm{d}u'_{\pi_s} = A_s \exp(-b_s u'_{\pi_s^+})$

In Fig.7 we display the distributions $\mathrm{d}\sigma/\mathrm{d}p_\perp^2$ where $p_\perp$ is transversal momentum of the centrally produced meson. The distributions show an exponential behaviour and are fitted with the form $\mathrm{d}\sigma/\mathrm{d}p_\perp^2 = A_c \exp(b_c p_\perp^2)$, the fit parameters A_c and b_c are given in Table 2.

6. Angular distributions

We have analyzed the angular distributions of the meson decay products in the Gottfried-Jackson frame, defined in the $\pi^+\pi^-$ c.m. system as follows. The Z-axis has been taken along the $(\vec{p}_{beam} - \vec{p}_{p_f})$ direction (the direction of momentum of the exchanged particle emitted from the upper vertex of diagram in Fig. 1b). The Y-axis has been taken as the normal to the production plane formed by the momentum of the virtual particle emitted from the upper

vertex and the slow pion one. Before plotting the angular distributions they were corrected for the trigger and Ω spectrometer acceptances. Then we have fitted the distributions using the formulae given in Refs. [3] and [6]. The fitted curves are shown in Fig.8, and the values for the density matrix elements are given in Table 3.

7. Comparison with the central production of mesons proceeding via boson exchange

Together with the investigation of ρ^0, f_2, ρ_3^0 central production via baryon exchange (i.e. in kinematics which can be designated as fast proton kinematics), we have analyzed the data of the WA56 to extract the similar production proceeding via boson exchange, i.e. the processes

$$\pi^+ p \to \pi_f^+ M^0 p_s \tag{4}$$

from the reaction with a fast pion kinematics

$$\pi^+ p \to \pi_f^+ \pi^+ \pi^- p_s \tag{5}$$

The events of reaction (5) were detected by the WA56 experimental set up with the same conditions as those of reaction (2). Among these conditions was the veto of π_f^+ that suppressed boson exchange reactions at the trigger level. However, due to some inefficiency of the veto, a part of events of reaction (5) was registered. Owing to the large cross section of reaction (5), the sample of these events turned out to be large enough. Fig. 9 presents MM^2 distributions of events having a $++-$ topology with a pion mass hypothesis for all detected particles. The peak at $\mathrm{MM}^2 = m_p^2$ corresponding to the events of reaction (5) is clearly seen. To select these events we imposed the cut $|\mathrm{MM}^2 - m_p^2| \leq 0.16$ $(\mathrm{GeV/c^2})^2$ followed by a 1-C fit procedure quite similarly to the selection of reaction (2).

In Fig. 10a the distribution of $\pi_f^+\pi^-$ mass is plotted displaying a strong ρ^0 and clear f_2 peaks. On the contrary, ρ^0 and f_2 signals in the mass distribution of the centrally produced $\pi^+\pi^-$ system given in Fig. 10b are weak.

The y^* distributions of $\pi_f^+, \pi^+\pi^-$ system and p_s are plotted in Fig. 5b. A good separation in rapidity is seen similar to that in the reaction (1). The events which have $|y^*_{\pi^+\pi^-}| \leq 0.5$ give the $\pi^+\pi^-$ mass spectrum shown in Fig. 10c. The ρ^0 and f_2 signal/background ratios are as low as in Fig. 10b. The comparison of Figs. 4a,b and 10b,c demonstrates prominent difference in the mass spectra of the $\pi^+\pi^-$ system produced centrally via baryon and boson exchanges.

We have checked that this difference does not originate from the bias caused by the selection of the π_f^+ events (the sample of the π_f^+ channel was enriched with events having a π_f^+ traversing the Cherenkov counters in the median plane, where the mirror edges caused

a local inefficiency, i.e. with π_f^+ having small $p_\perp$). The events with a π_f^+ having $p_\perp$ greater than 300 MeV/c give similar $\pi^+\pi^-$ mass distributtions as those shown in Fig. 10b, 10c.

The smallness of the signal/background ratio for mesons produced centrally in the fast pion kinematics can be understood in terms of Regge-trajectory exchange. The common feature of reactions like (5) is the abundance of forward meson production since pion exchange (which is intense) is allowed here (the corresponding diagram is shown in Fig. 11). Our experimental data illustrates this feature, see Fig. 10a. On the contrary, pion exchange is forbidden in central production of mesons (see Fig. 1a). As a result, the signals of centrally produced mesons are small and are weakly seen in our data, being faked by the large background originating from the forward production channels.

Concerning baryon exchange processes, their relative yilds are expected to be of the same order since all these processes proceed through the exchange of baryonic singularities. From this point of view we could expect approximately equal cross sections for meson central production as compared to the typical backward production ones in the fast proton kinematics. Indeed, we observe a weak prevalence of ρ^0 and f_2 central production over backward production of the same mesons associated with $\Delta(1232)$ (analyzed in [3]):

$$\frac{\sigma(\pi^+p \to p_f\rho^0\pi_s^+)}{\sigma(\pi^+p \to \Delta_f^{++}\rho^0)} \approx 4, \tag{6}$$

$$\frac{\sigma(\pi^+p \to p_f f_2\pi_s^+)}{\sigma(\pi^+p \to \Delta_f^{++}f_2)} \approx 3 \tag{7}$$

The conclusion which can be drawn from the comparison of the central production of mesons in the fast proton and the fast pion kinematics is that the former is very suitable for the hadron spectroscopy providing good signal/background ratios. In particular, various exotic states including baryonium could be investigated in this kinematical domain.

8. Conclusions

We have studied for the first time the central production of mesons in baryon exchange processes. The quasi-three-body reactions $\pi^+p \to p_f\rho^0\pi_s^+$, $\pi^+p \to p_f f_2\pi_s^+$, and $\pi^+p \to p_f\rho_3^0\pi_s^+$ were identified using the WA56 data obtained at the CERN Ω spectrometer. We have obtained the integral and differential cross sections for these channels and the density matrix elements of centrally produced mesons. From our analysis we conclude that the processes of vector and tensor meson central production in baryon exchange reactions are very clean being observed with a high signal/background ratio.

Acknowledgements

We are indebted to the WA56 Collaboration for allowing us to analyze the data of their experiment. A.A.G. and V.F.P. would like to express their gratitude to the IFIC for kind hospitality and help during preparation of this paper. We thank K.G.Boreskov, A.B.Kaidalov for many useful discussions, and N.Z.Akopov, F.Alted, V.I.Mikhailichenko for their assistance.

References

[1] T.A.Armstrong *et al.,* Phys. Lett. 227B (1989) 186

[2] Z. Ajaltouni *et al.,* Nucl. Phys. B209 (1982) 301.

[3] V.F.Perepelitsa et al., CERN-PPE/90-164. To be published in Z. Phys. C.

[4] J.K. Storrow, Phys. Rep. 103 (1984) 317.

[5] PDG, Review of Particle Properties, Phys. Lett. 239B (1990) 1.

[6] J.D. Jackson, Nuovo Cim. 34 (1964) 1644.

Table Captions

Table 1. Number of events, acceptances and integral cross sections for reaction (1) with centrally produced ρ^0, f_2 and ρ_3^0 mesons.

Table 2. $d\sigma/du'$ and $d\sigma/dp_\perp^2$ parameters for reaction (1) with centrally produced ρ^0, f_2 and ρ_3^0 mesons.

Table 3. Density matrix elements of centrally produced ρ^0, f_2 and ρ_3^0 mesons.

Figure Captions

Fig. 1) The diagrams which correspond to the central production of a mesonic state M^0 in π^+p interactions via a) boson and b) baryon exchange mechanisms. P stands for Pomeron Regge trajectory, α_M (α_B) denotes the meson (baryon) Regge trajectories ($M = \pi, \rho, f, A_2, \ldots$; $B = N, \Delta$), and subscripts f, s designate the fastest and the slowest particles in the reaction.

Fig. 2) The layout of the Ω spectrometer as used in the WA56 experiment.

Fig. 3) MM^2 distributions for $\pi^+p \to p_f\pi^+\pi^-(MM)$ hypothesis for 3-prong $++-$ events: a) all events and b) events with the missing momentum extrapolating to the fired barrel element. The dashed vertical lines give the MM^2 limits of accepted events as input to the kinematics fitting program.

Fig. 4) Spectra of $\pi^+\pi^-$ mass of events from the reaction $\pi^+p \to p_f\pi^+\pi^-\pi_s^+$: a) all events; b) events with $y^*_{\pi^+\pi^-}$ in the range from -0.5 to $+0.5$; c) events with the additional cut $M(p_f\pi^+) \geq 2$ GeV/c^2. The curves are the mass fit results explained in the text.

Fig. 5) Rapidity distributions: a) for the reaction $\pi^+p \to p_f\pi^+\pi^-\pi_s^+$; b) for the reaction $\pi^+p \to \pi_f^+\pi^+\pi^-p_s$ (see the text, Chapt.7).

Fig. 6) Differential cross sections $d\sigma/du'$ of reactions $\pi^+p \to p_f\rho^0\pi_s^+$ (a,b); $\pi^+p \to p_f f_2\pi_s^+$ (c,d); and $\pi^+p \to p_f\rho_3^0\pi_s^+$ (e,f).

Fig. 7) Differential cross sections $d\sigma/dp_\perp^2$ of reactions $\pi^+p \to p_f\rho^0\pi_s^+$ (a); $\pi^+p \to p_f f_2\pi_s^+$ (b); and $\pi^+p \to p_f\rho_3^0\pi_s^+$ (c).

Fig. 8) $\cos(\theta)$ and ϕ angles of the M^0 decay products in the Jackson frame determined as described in the text, for reactions $\pi^+p \to p_f\rho^0\pi_s^+$ (a,b); $\pi^+p \to p_f f_2\pi_s^+$ (c,d); and $\pi^+p \to p_f\rho_3^0\pi_s^+$ (e,f).

Fig. 9) MM^2 distributions for $\pi^+p \to \pi_f^+\pi^+\pi^-(MM)$ hypothesis for 3-prong $+ + -$ events: a) all events and b) events with the missing momentum extrapolating to the fired barrel element. The dashed vertical lines give the MM^2 limits of accepted events as input to the kinematics fitting program.

Fig. 10) Mass spectra for events from reaction $\pi^+p \to \pi_f^+\pi^+\pi^-p_s$: a) $\pi_f^+\pi^-$ mass; b)$\pi^+\pi^-$ mass, all events; c)$\pi^+\pi^-$ mass, events with $y^*_{\pi^+\pi^-}$ in the range from -0.5 to $+0.5$. The curves are the mass fit results explained in the text.

Fig. 11) The diagram which corresponds to the forward production of a mesonic state M^0 in π^+p interactions via boson exchange.

Table 1: Number of events, acceptances and integral cross sections for reaction (1) with centrally produced ρ^0, f_2 and ρ_3^0 mesons.

Channel	Number of events (background subtracted)	Acceptance (%)	σ_{int} (nb)
$\pi^+p \to p_f\rho^0\pi_s^+$	1200 ± 80	7.2	110 ± 10
$\pi^+p \to p_f f_2\pi_s^+$	1200 ± 70	7.0	210 ± 20
$\pi^+p \to p_f\rho_3^0\pi_s^+$	140 ± 30	3.2	120 ± 30

Table 2: $d\sigma/du'$ and $d\sigma/dp_1^2$ parameters for reaction (1) with centrally produced ρ^0, f_2 and ρ_3^0 mesons.

Channel	Normalization	coefficients (nb)	Slopes	$(\text{GeV/c})^{-2}$
$\pi^+p \to p_f\rho^0\pi_s^+$	$A_f = 212 \pm 9$ $A_{s_1} = 470 \pm 32$ $A_{s_2} = 180 \pm 50$	$A_c = 239 \pm 10$	$b_f = 2.0 \pm 0.1$ $b_{s_1} = 6.6 \pm 0.6$ $b_{s_2} = 2.1 \pm 0.2$	$b_c = 2.1 \pm 0.1$
$\pi^+p \to p_f f_2\pi_s^+$	$A_f = 396 \pm 17$ $A_{s_1} = 716 \pm 43$ $A_{s_2} = 196 \pm 70$	$A_c = 396 \pm 16$	$b_f = 1.8 \pm 0.1$ $b_{s_1} = 5.0 \pm 0.5$ $b_{s_2} = 1.6 \pm 0.3$	$b_c = 1.9 \pm 0.1$
$\pi^+p \to p_f\rho_3^0\pi_s^+$	$A_f = 179 \pm 21$ $A_s = 224 \pm 29$	$A_c = 196 \pm 22$	$b_f = 1.6 \pm 0.2$ $b_s = 2.3 \pm 0.3$	$b_c = 1.7 \pm 0.2$

Table 3: Density matrix elements of centrally produced ρ^0, f_2 and ρ_3^0 mesons.

Reaction $\pi^+ p \to p_f \rho^0 \pi_s^+$

$$\rho_{00} = 0.34 \pm 0.02 \qquad \rho_{1-1} = -0.03 \pm 0.02$$
$$\rho_{11} = 0.33 \pm 0.01 \qquad Re\rho_{10} = -0.01 \pm 0.01$$

Reaction $\pi^+ p \to p_f f_2 \pi_s^+$

$$\rho_{00} = 0.33 \pm 0.05 \qquad Re\rho_{20} = 0.00 \pm 0.01$$
$$\rho_{11} = 0.22 \pm 0.02 \qquad \rho_{2-2} = 0.00 \pm 0.02$$
$$\rho_{22} = 0.12 \pm 0.02 \qquad Re\rho_{21} = 0.01 \pm 0.01$$
$$\rho_{1-1} = -0.04 \pm 0.02 \qquad Re\rho_{10} = -0.03 \pm 0.01$$
$$Re\rho_{2-1} = -0.01 \pm 0.01$$

Reaction $\pi^+ p \to p_f \rho_3^0 \pi_s^+$

$$\rho_{00} = 0.32 \pm 0.07 \qquad \rho_{1-1} + 2/\sqrt{15} Re\rho_{31} + \sqrt{6/5} Re\rho_{20} =$$
$$\rho_{11} = 0.26 \pm 0.02 \qquad = -0.17 \pm 0.04$$
$$\rho_{22} = 0.09 \pm 0.02 \qquad \rho_{2-2} + 2/\sqrt{15} Re\rho_{3-1} = 0.02 \pm 0.04$$
$$\rho_{33} = -0.01 \pm 0.02 \qquad \rho_{3-3} = 0.01 \pm 0.05$$

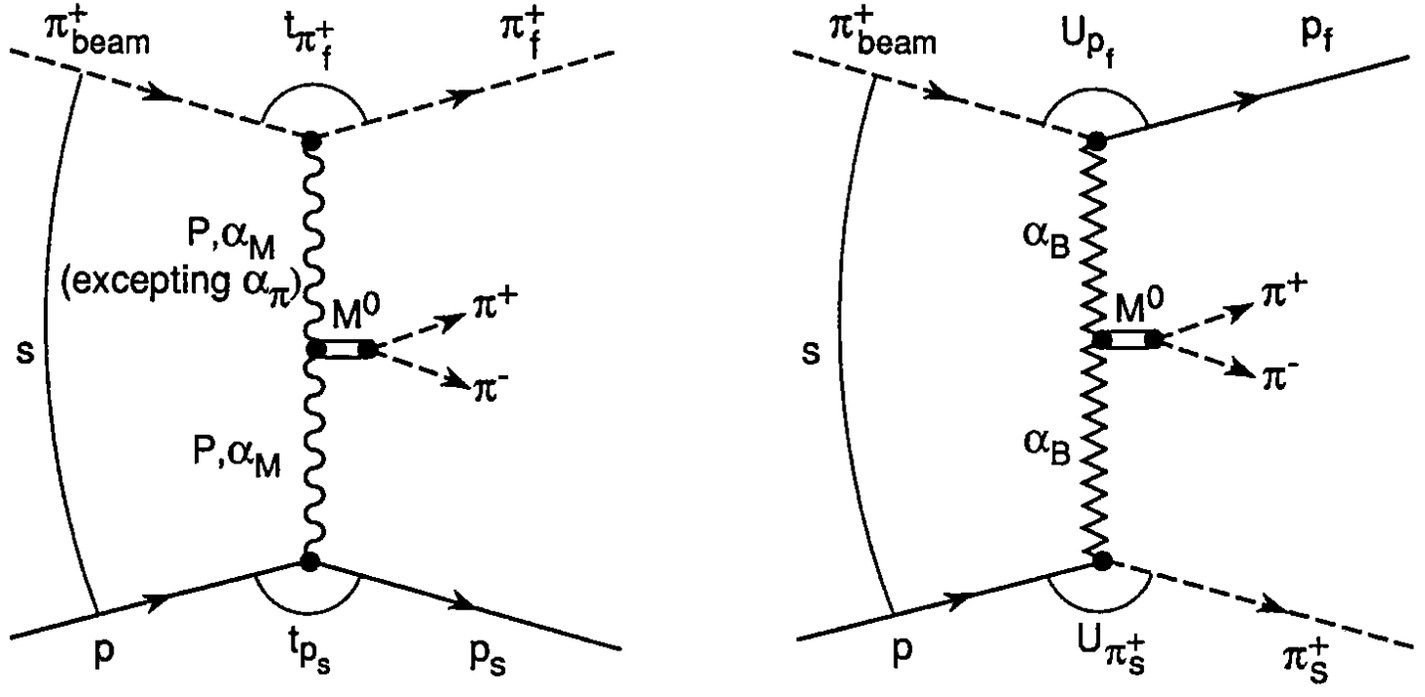
π^+_{beam}
$t_{\pi^+_f}$
π^+_f
P,α_M
(excepting α_π)
M^0
π^+
π^-
s
P,α_M
p
t_{p_s}
p_s
a)
π^+_{beam}
U_{p_f}
p_f
α_B
M^0
π^+
π^-
s
α_B
p
$U_{\pi^+_s}$
π^+_s
b)

FIG. 1

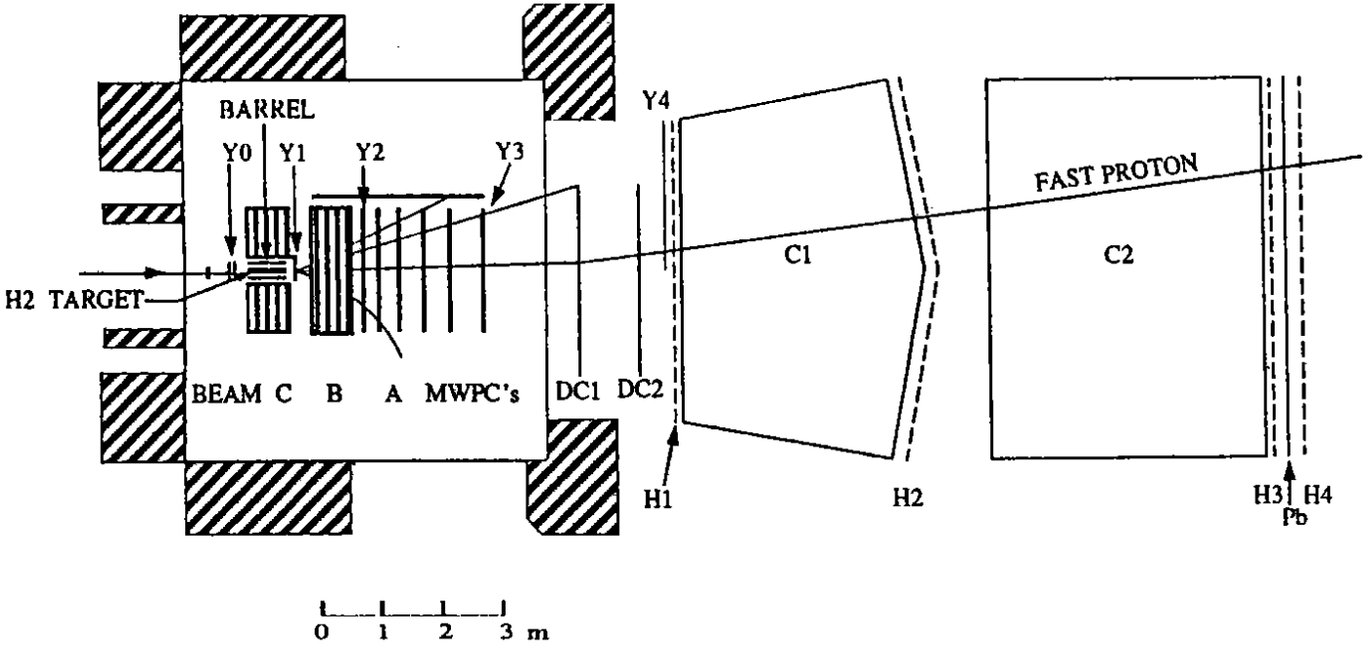
BARREL
Y0
Y1
Y2
Y3
Y4
FAST PROTON
H2 TARGET
C1
C2
BEAM C
B
A
MWPC's
DC1
DC2
H1
H2
H3
H4
Pb
0
1
2
3 m

FIG. 2

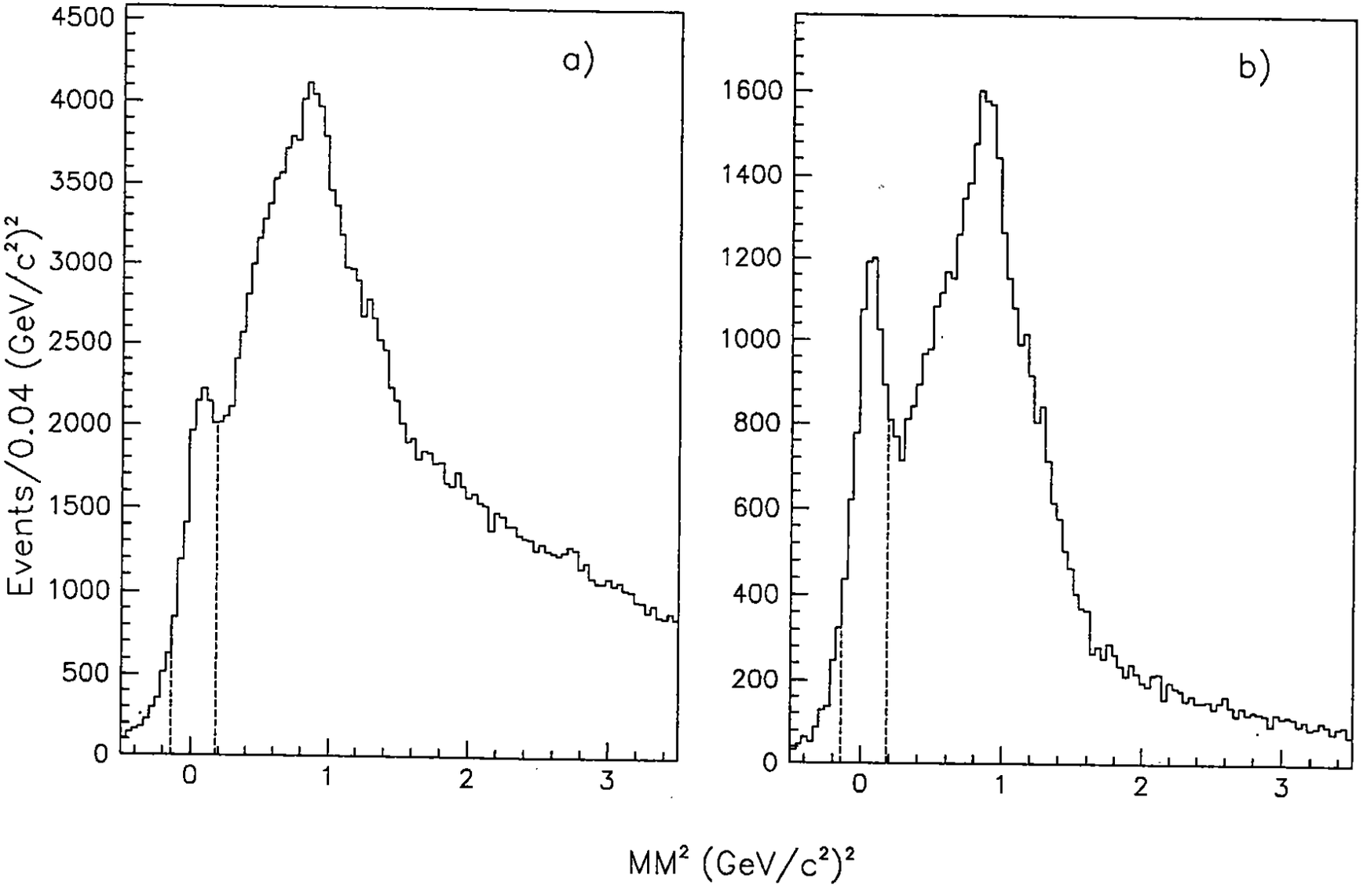
a)
b)
Events/0.04 (GeV/c²)²
MM² (GeV/c²)²
4500
4000
3500
3000
2500
2000
1500
1000
500
0
1600
1400
1200
1000
800
600
400
200
0
1
2
3

FIG. 3

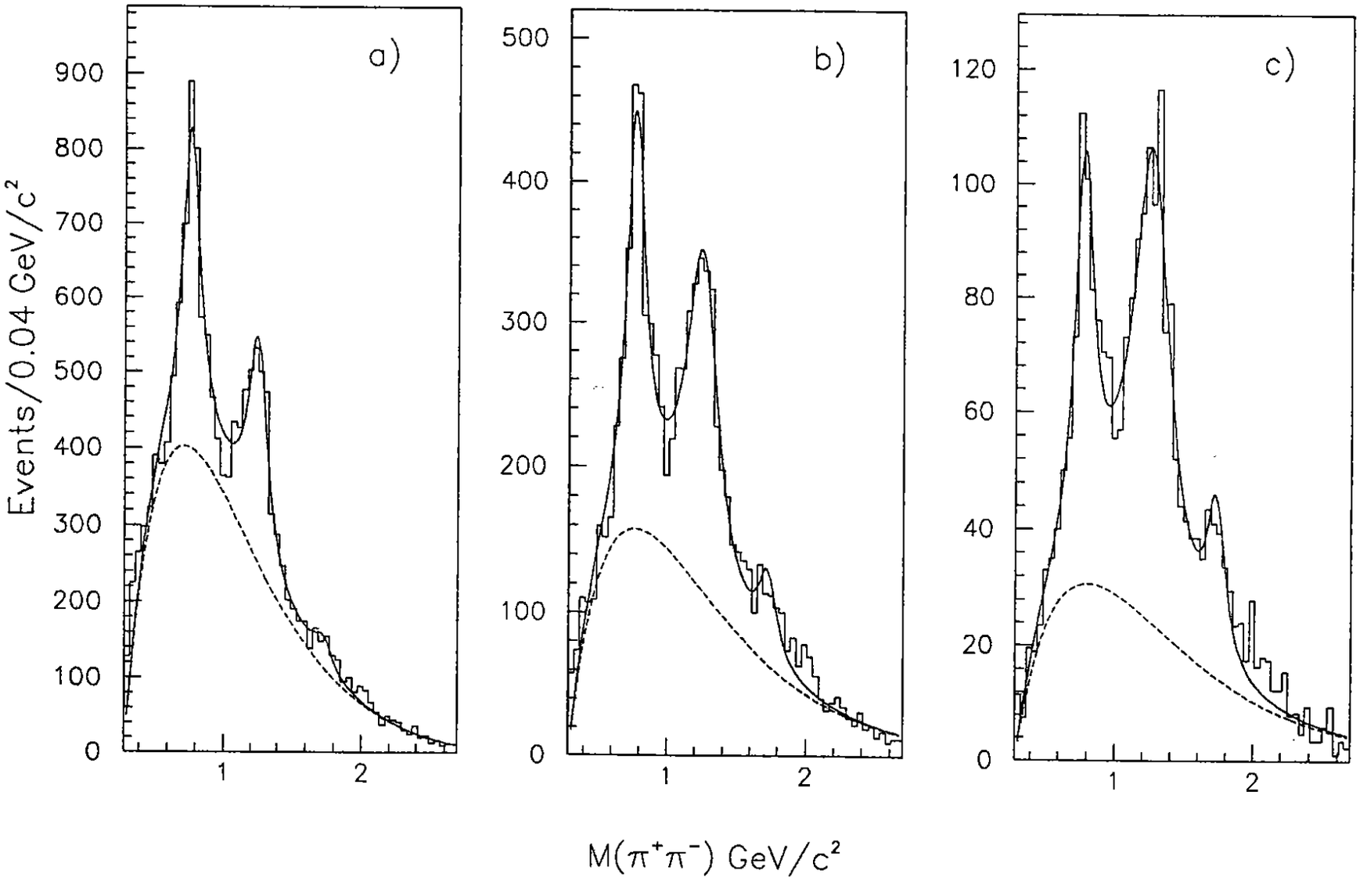
a)
b)
c)
Events/0.04 GeV/c²
M(π⁺π⁻) GeV/c²
0
100
200
300
400
500
600
700
800
900
20
40
60
80
100
120
1
2

FIG. 4

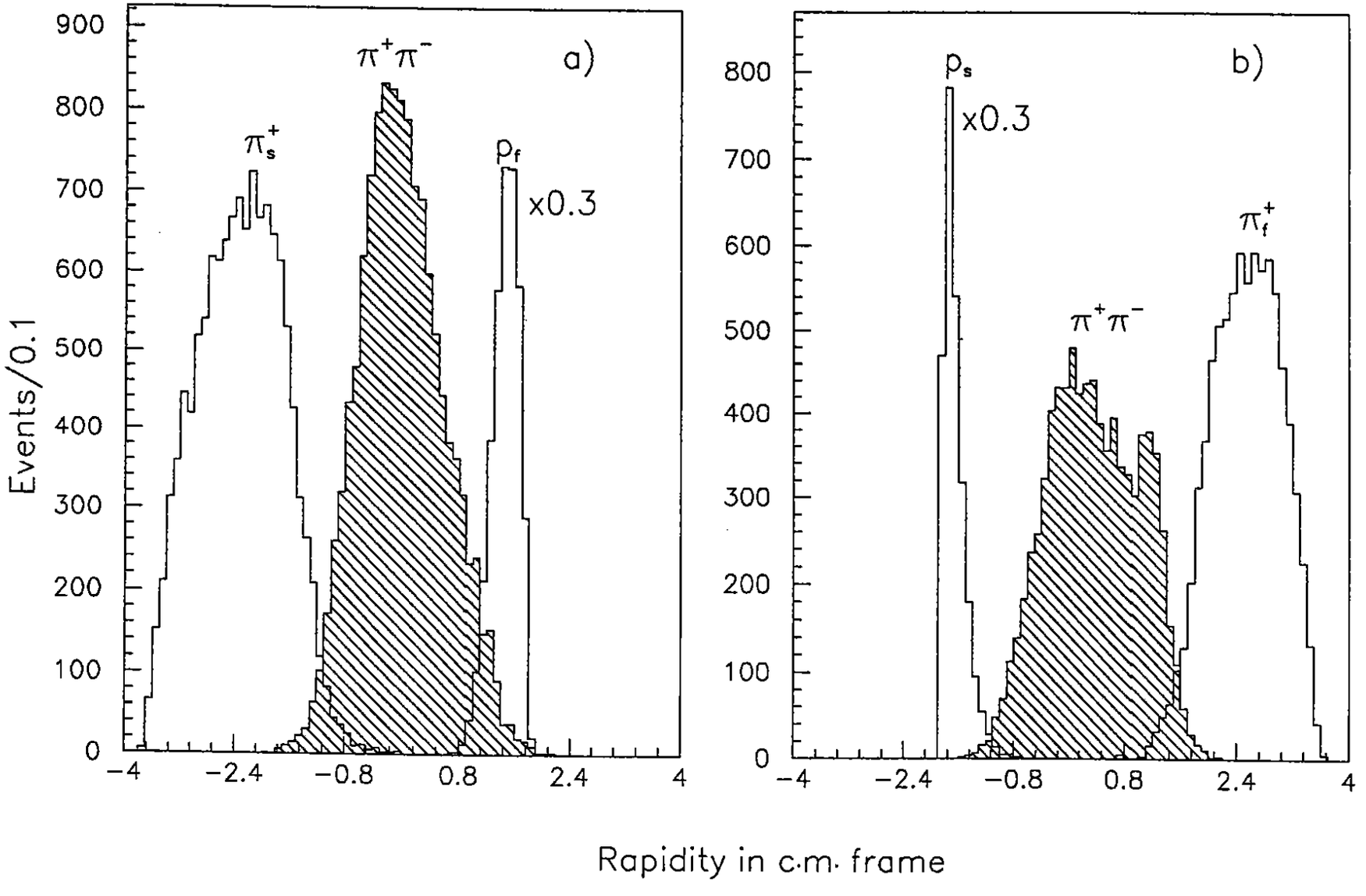
Events/0.1
900
800
700
600
500
400
300
200
100
0
−4
−2.4
−0.8
0.8
2.4
4
$\pi^+\pi^-$
a)
π_s^+
p_f
x0.3
800
700
600
500
400
300
200
100
0
p_s
x0.3
b)
π_f^+
$\pi^+\pi^-$
Rapidity in c.m. frame

FIG. 5

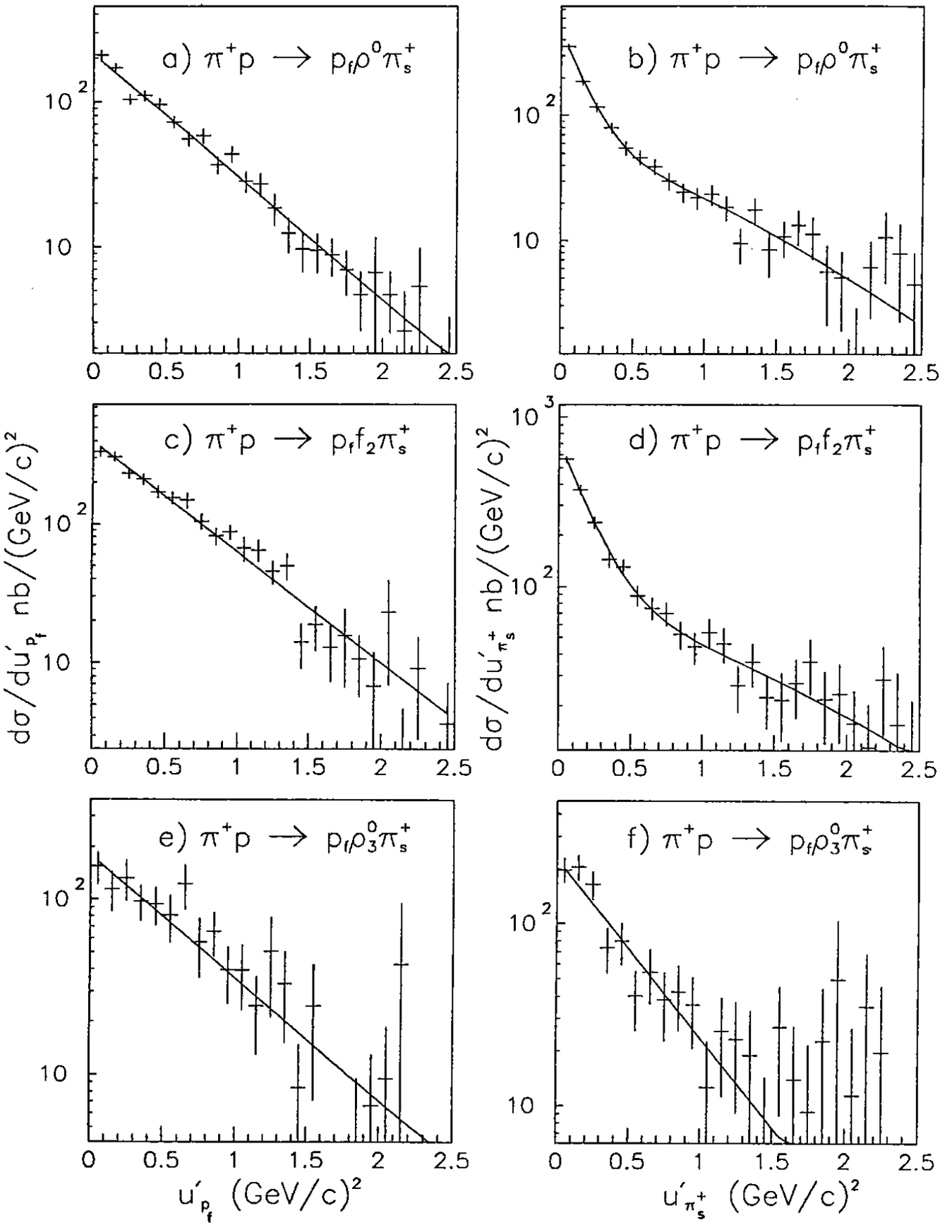
a) $\pi^+p \rightarrow p_f\rho^0\pi_s^+$
b) $\pi^+p \rightarrow p_f\rho^0\pi_s^+$
c) $\pi^+p \rightarrow p_f f_2\pi_s^+$
d) $\pi^+p \rightarrow p_f f_2\pi_s^+$
e) $\pi^+p \rightarrow p_f\rho_3^0\pi_s^+$
f) $\pi^+p \rightarrow p_f\rho_3^0\pi_s^+$
$d\sigma/du'_{p_f}$ nb/(GeV/c)^2
$d\sigma/du'_{\pi_s^+}$ nb/(GeV/c)^2
u'_{p_f} (GeV/c)^2
$u'_{\pi_s^+}$ (GeV/c)^2

FIG. 6

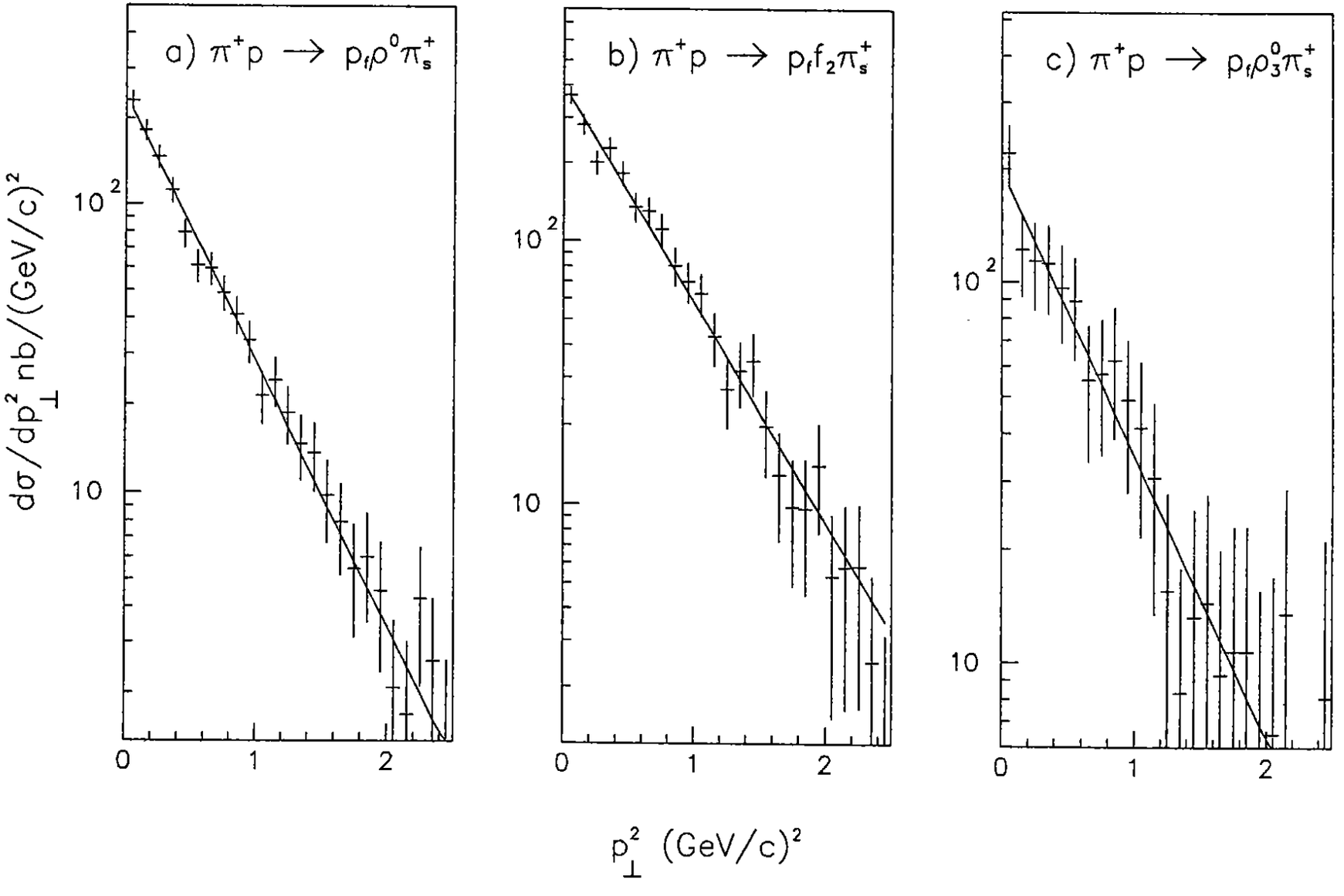
a) $\pi^+ p \rightarrow p_f \rho^0 \pi_s^+$
b) $\pi^+ p \rightarrow p_f f_2 \pi_s^+$
c) $\pi^+ p \rightarrow p_f \rho_3^0 \pi_s^+$
$d\sigma/dp_\perp^2$ nb/(GeV/c)^2
10^2
10
0
1
2
$p_\perp^2$ (GeV/c)^2

FIG. 7

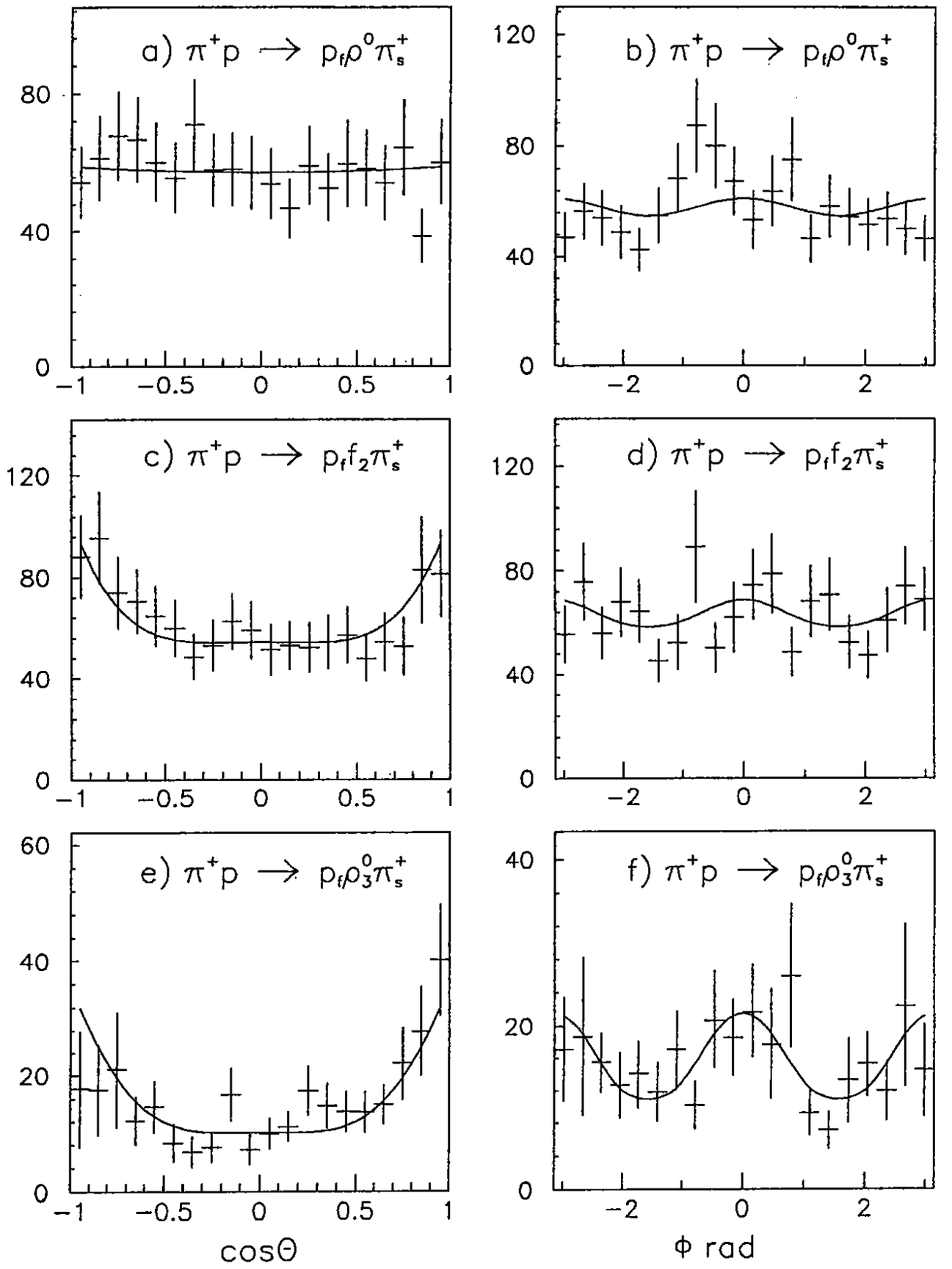
a) $\pi^+ p \rightarrow p_f \rho^0 \pi_s^+$
b) $\pi^+ p \rightarrow p_f \rho^0 \pi_s^+$
c) $\pi^+ p \rightarrow p_f f_2 \pi_s^+$
d) $\pi^+ p \rightarrow p_f f_2 \pi_s^+$
e) $\pi^+ p \rightarrow p_f \rho_3^0 \pi_s^+$
f) $\pi^+ p \rightarrow p_f \rho_3^0 \pi_s^+$
cosΘ
Φ rad

FIG. 8

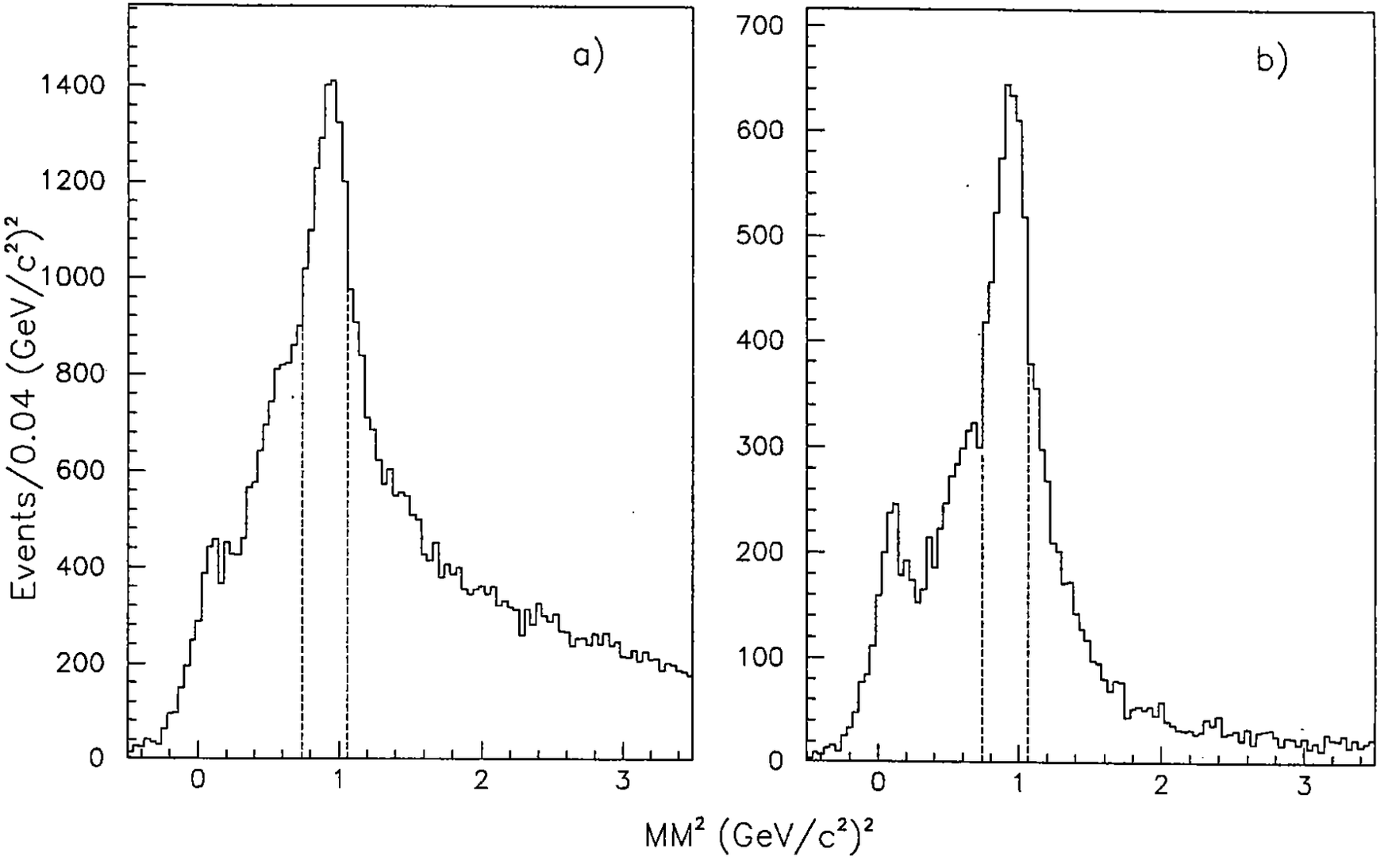
a)
b)
Events/0.04 (GeV/c²)²
MM² (GeV/c²)²
0
200
400
600
800
1000
1200
1400
100
300
500
700
1
2
3

FIG. 9

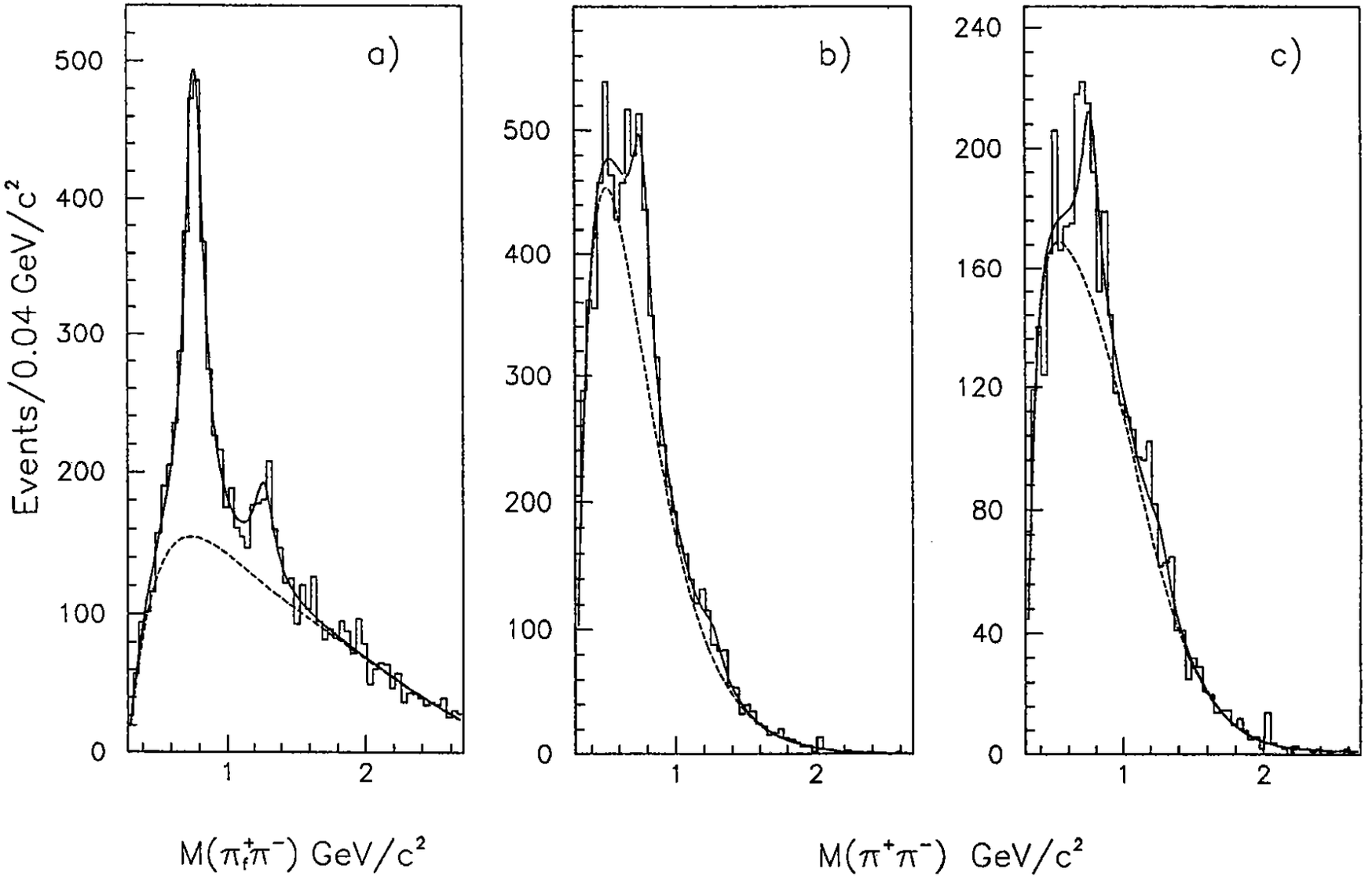

FIG.10

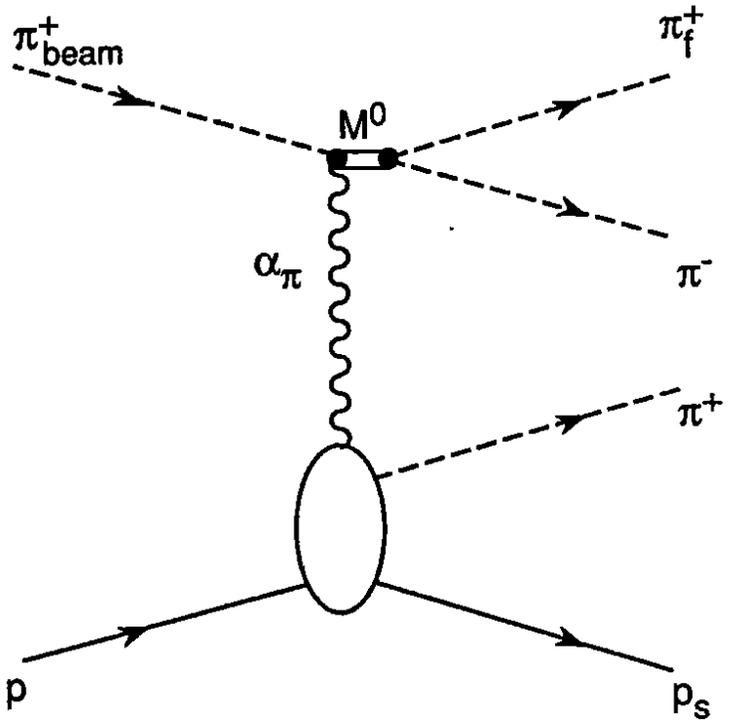

FIG. 11

Imprimé au CERN. Prix: 0.70 Fr.